A Hybrid Calibration-Free/Artificial Neural Networks Approach to the Quantitative Analysis of LIBS Spectra

Eleonora D'Andrea[1], Stefano Pagnotta[2], Emanuela Grifoni[2], Stefano Legnaioli[2], Giulia Lorenzetti[2], Vincenzo Palleschi[2], Beatrice Lazzerini[1]

[1] Department of Information Engineering, University of Pisa
Largo Lucio Lazzarino 1, 56122 Pisa (ITALY)

[3] Institute of Chemistry of Organometallic Compounds
Research Area of National Research Council, Via G. Moruzzi, 1 – 56124 Pisa (ITALY)

ABSTRACT

A 'hybrid' method is proposed for the quantitative analysis of materials by LIBS, combining the precision of the Calibration-Free LIBS (CF-LIBS) algorithm with the quickness of Artificial Neural Networks. The method allows the precise determination of the samples' composition even in the presence of relatively large laser fluctuations and matrix effects. To show the strength and robustness of this approach, a number of synthetic LIBS spectra of Cu-Ni binary alloys with different composition were computer-simulated, in correspondence of different plasma temperatures, electron number densities and ablated mass. The CF-LIBS/ANN approach here proposed demonstrated to be capable, after appropriate training, of 'learning' the basic physical relations between the experimentally measured line intensities and the plasma parameters. Because of that, the composition of the sample can be correctly determined, as in CF-LIBS measurements, but in a much shorter time.

Keywords: Artificial Neural Networks, Laser-Induced Breakdown Spectroscopy, Cu-Ni alloys, Quantitative Analysis, Simulation

Corresponding Author:

Vincenzo Palleschi
e-mail: vincenzo.palleschi@cnr.it
WWW: http://www.alslab.net

1.– Introduction

The use of Artificial Neural Networks (ANNs) [1-2] in Laser-Induced Breakdown Spectroscopy (LIBS) [3-4] quantitative analysis has been recently proposed in several research papers [5-9], because of the quickness and robustness of the algorithms and the availability of specialized commercial and open-source software [10]. The idea at the basis of most of the ANNs applications to the analysis of LIBS spectra is, in fact, the construction of non-linear combination of a given number of inputs (LIBS spectral intensities), optimized for obtaining the best representation of a set of outputs (elemental concentrations) on a number of known samples (training). The coefficients of this multivariate, non-linear combination, after a proper validation and testing can be used for calculating the desired outputs from a set of inputs obtained on unknown samples (prediction).
A reason of the success of ANNs in LIBS analysis is the extreme facility by which is possible, in a LIBS experiment, to accumulate hundreds of spectra, thus providing a quite large database for the most critical steps of the ANN procedure, i.e. the training and validation of the ANN model [11].
On the other hand, the ANN approach has important limitations that in some cases are similar to the one encountered in linear multivariate analysis [12] or even in standard monovariate analysis (calibration curves) [13].
In fact, one can intend the training of the network in a manner similar to the construction of a (multidimensional and non-linear) calibration curve (which eventually becomes a surface in a multidimensional parameters' space).
For linking effectually a series of 'inputs' to the 'outputs' (in a LIBS application, one can think about spectral lines' intensities as inputs, and elemental concentration as outputs) one should bring in mind that the general rules for the building of calibration curves [14] hold also for the ANN approach, i.e.:

Rule 1 – The experimental conditions in which the 'calibration' spectra are acquired must be the same through all the calibration process, and must be maintained constant during the acquisition of the LIBS spectra on the unknown samples;
Rule 2 – The methods based on a calibration approach are good for interpolation but might fail when used for extrapolating data out of the range of the calibration set. In other words, it is advisable that the samples used for training the ANN would bracket the concentrations of the unknown samples.

These two requirements put, obviously, important constraints on the applicability of the ANN method for the analysis of LIBS spectra that, by their nature, are extremely variable in response to changes, either intentional or unwanted, in the physical parameters of the plasma, i.e. ablated mass, electron number density and electron temperature. In LIBS experiments, the variation of the experimental parameters during the measurement is often unwanted but almost unavoidable, because of the laser energy fluctuations and the matrix changes between one sample and the other. To overcome the limitation of the classical calibration approach, either monovariate or multivariate, the authors proposed several years ago a method called Calibration-Free LIBS [15-18], which is based on the possibility of measuring the above parameters, by which the atomic emission is governed, with the aim of obtaining outputs (concentrations) which would not depend on the fluctuations in laser energy and coupling with the target. In fact, these fluctuations are the main responsible for the variation of ablated mass, plasma temperature and electron number density and, in the last instance, for the indetermination in the relation between the inputs (line intensities) and the outputs, which is reflected in a corresponding indetermination on the calibration curve or the ANN model to be used for the determination of the composition of the unknown samples.
In a recent paper [19], the authors demonstrated the possibility of integrating the information obtained from the CF-LIBS method with the ANN algorithm, proposing a fast method for measuring electron temperature and number density on a pure Titanium target, at the varying of the laser beam fluence on the target.
In this paper, we will demonstrate that using an approach based on the same concept the composition of a metallic alloy can be determined even when the Rules described above are not followed, providing a result which is much more precise than the one that can be obtained using the calibration curves approach and much faster than the one obtained by the use of the CF-LIBS approach, with a similar precision.

2 – Experimental approach

For obtaining a better understanding of the advantages of an approach with respect to the others, we decided to work on synthetic LIBS spectra, simulated using a software developed by the authors [20]. The software is able to reproduce a number of complex experimental plasma (multi-elemental, inhomogeneous, subject to self-absorption and with temperature and electron number density gradients) but, for the present application, the LIBS spectra of a simple

binary alloy (Cu-Ni) were simulated, assuming a homogeneous plasma at a given constant temperature and electron number density, with negligible self-absorption effects.

We considered an ideal set of samples, with Ni concentrations ranging from 0 to 10 percent, analyzed by LIBS in different experimental conditions, roughly corresponding to the use of laser energies varying from 50 to 150 mJ in a typical LIBS configuration (1064 nm laser wavelength, 10 ns pulse width, 200 μm laser spot on the target). These data were chosen to mimic the results of a real experiment (not shown here) from where realistic values of the parameters used in the simulation (electron temperature and number densities, ablated mass) were derived.

The experimental configurations considered to generate this set of data are summarized in Table I.

Table I – Parameters used for the generation of the synthetic LIBS spectra: Ni concentrations, electron temperature, and electron number density corresponding to the three simulated laser energies

Sample	Laser Energy	[Ni] (%)	T (eV)	n_e (cm^{-3})
S1	50	0	1.1	$3x10^{16}$
S2	50	2	1.1	$3x10^{16}$
S3	50	5	1.1	$3x10^{16}$
S4	50	10	1.1	$3x10^{16}$
S5	100	0	1.2	$3.5x10^{16}$
S6	100	3	1.2	$3.5x10^{16}$
S7	100	5	1.2	$3.5x10^{16}$
S8	100	8	1.2	$3.5x10^{16}$
S9	100	10	1.2	$3.5x10^{16}$
S10	150	0	1.25	$4x10^{16}$
S11	150	2	1.25	$4x10^{16}$
S12	150	5	1.25	$4x10^{16}$
S13	150	10	1.25	$4x10^{16}$

The ablated mass was considered proportional to the electron density.

The most intense emission lines of Cu and Ni, as experimentally observed in real LIBS experiments in the wavelength range between 200 and 500 nm, were simulated. The corresponding central wavelengths are shown in Table II.

Table II – Spectral parameters of the lines considered

Species	Wavelength (nm)	g_k	E_k (cm^{-1})	A_{ki} (s^{-1})
Ni II	241.6	8	$5.64 \cdot 10^4$	$2.10 \cdot 10^8$
Ni II	251.1	10	$5.34 \cdot 10^4$	$0.58 \cdot 10^8$
Cu I	330.8	12	$7.11 \cdot 10^4$	$2.22 \cdot 10^8$
Ni I	349.3	3	$2.95 \cdot 10^4$	$0.98 \cdot 10^8$
Ni I	362.0	7	$3.1 \cdot 10^4$	$0.66 \cdot 10^8$
Cu I	521.8	6	$4.99 \cdot 10^4$	$1.22 \cdot 10^8$
Cu I	578.2	2	$3.05 \cdot 10^4$	$0.02 \cdot 10^8$

In Table II the symbols 'I' and 'II' refer to the neutral and singly ionized species of the element, respectively. The equations used for the generation of the synthetic spectra were based on the Local Thermal Equilibrium approximation [21]: the Boltzmann equation, which links the intensities of the lines emitted by the same species:

$$I_k = F\, C^{(I,II)} \frac{A_{ki} g_k}{U^{(I,II)}(T)} e^{-\frac{E_k}{kT}} \qquad (1)$$

and the Saha-Boltzmann equation, which links the concentrations of the two different ionization stages of the same element:

$$\frac{n_e C^{II}}{C^I} = \frac{(2\pi m_e kT)^{3/2}}{h^3} \frac{2U^{II}(T)}{U^I(T)} \exp(-\frac{E_{ion}}{kT}) \qquad (2)$$

In equations (1) and (2), *F* is a factor, proportional to the ablated mass, which in real experiments also takes into account the (constant) efficiency of the spectral detection system, *T* represents the electron temperature, n_e is the electron number density, *N* is the concentration of the species, E_k and E_{ion} are the energies of the upper level of the transition and the ionization energy of the element, respectively, A_{ki} and g_k are the transition probability and the degeneracy of the upper level, tabulated in the NIST database [22], $U(T)$ is the partition function of the species considered, *k* is the Boltzmann constant, m_e is the electron mass and *h* is the Planck constant. We assumed, as usual in LIBS measurements, that $C^I + C^{II} = C_s$, where C_s represents the concentration of the element in the sample. The variability between the spectra was simulated by applying a random Poisson noise at each considered wavelength, with λ value equal to the average value of the emission intensity at that wavelength. Then, 1000 independent spectra were simulated for each 'sample' in Table I at the different laser energies.

3 – Quantitative analysis of the synthetic LIBS spectra

3.1 Calibration-free analysis

Since the simulated LIBS spectra were obtained using the basic LTE equation in ideal conditions (homogeneous plasma, no self-absorption effects), the application of the CF-LIBS method, which is based on exactly the same assumptions, would give a perfect agreement between the nominal concentrations and the ones determined by the analysis. In principle, the CF-LIBS is able to take into account the unavoidable variations in laser energy and coupling with the sample on a single spectrum basis, but this possibility is seldom exploited in practice, since in a real experimental condition the application of the method on thousands of samples would take a prohibitively long time. The approach generally used in CF-LIBS analysis is working on averaged spectra, although it should be clear that the sample compositions calculated on an averaged spectrum could be different from the average of the compositions determined on the single spectra.

3.2 Calibration curve approach

A simpler approach to the quantitative analysis of a large number of spectra is the building of a suitable calibration curve by plotting the line intensity of one of the characteristic emission lines of the element vs. its known concentration in the sample. In the case of the LIBS simulated data that are the subject of our discussion, the calibration curve approach in correspondence of the three configurations considered, roughly corresponding to laser energies of 50, 100 and 150 mJ, produces, as it should, three different linear curves (see figure 1).

The effect of the variation of laser energy is often compensated, in the framework of the calibration curve approach, by plotting the ratio of the line intensity of the minor element of interest (in this case, Ni) to the line intensity of an element in the matrix (Cu), as a function of the concentration ratio. In our case, being the alloy binary, the two concentrations of Cu and Ni are related as [Ni]=100% - [Cu] , were the square brackets indicate the concentration of the element in percent. It is therefore very simple to obtain the individual concentrations of Ni and Cu once their ratio is known. However, this approach does not completely reduce the spread between the calibration curves obtained at the different energies, as evidenced in figure 2.

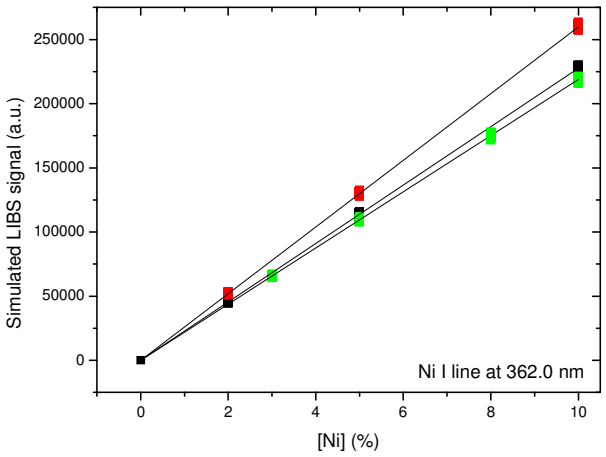

Fig. 1. Calibration curves for the samples analyzed at the laser energy of 50 mJ (black squares), 100 mJ (green squares) and 150 mJ (red squares).

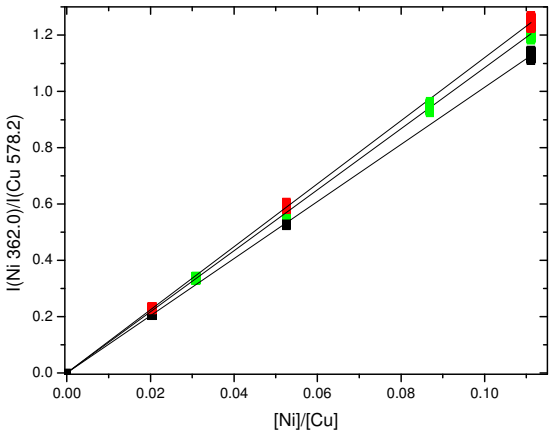

Fig. 2. Calibration curves for the samples analyzed at the laser energy of 50 mJ (black squares), 100 mJ (green squares) and 150 mJ (red squares). The intensity ratio between intensities of the Ni I line at 362.0 nm and the Cu I line at 578.2 nm is plotted versus the ratio of Ni and Cu concentrations.

In fact, the ratio of two lines of Ni and Cu can be written as

$$\frac{I_k^{Ni}}{I_k^{Cu}} = \frac{[NiI]}{[CuI]} \frac{A^{Ni}_{ki} g^{Ni}_{k} U^{Cu}(T)}{A^{Cu}_{ki} g^{Cu}_{k} U^{Ni}(T)} e^{-\frac{\left(E^{Cu}_{k} - E^{Ni}_{k}\right)}{kT}}. \qquad (3)$$

Neglecting the dependence on the temperature of the partition function $U(T)$, the only dependence on the electron temperature T of the line ratio of equation (3) is through the exponential, which becomes close to 1 when $E^{Cu}_{k} \approx E^{Ni}_{k}$. This is apparently the case of the lines considered in figure 2, where the Ni I line at 362.0 nm (E_k=3.1·10^4 cm^{-1}) is divided by the Cu I line at 578.2 nm (E_k=3.05·10^4 cm^{-1}). However, the Saha-Boltzmann equation (equation (2)) states that, even when $E^{Cu}_{k} \approx E^{Ni}_{k}$, the ratio between two lines of the same ionization stage is

proportional to the ratio between the concentrations of the two corresponding species, which is not the same as the ratio of the concentrations of the elements, because [Cu]=[Cu I]+[Cu II], [Ni]=[Ni I]+[Ni II] and the ratios [Ni II]/[Ni I] and [Cu II]/[Cu I] depend on the temperature differently for the two elements, according to the predictions of equation (2).

It is thus evident that a simple approach based on the building of a calibration curve would not allow for the quantitative analysis of LIBS spectra when both the Ni concentration and the laser irradiance on the sample are unknown.

3.3 Artificial Neural Network analysis

Artificial Neural Networks are data-driven intelligent systems with the capability to learn from examples. Based on suitable collected data, ANNs can be trained to approximate any input-output relationship with any desired degree of accuracy. We therefore decided to apply the neural network approach to the specific case under study in order to overcome the unsatisfactory results of the calibration curve approach. To this aim, we built a neural network using as output the Ni concentration of the samples, and as inputs the simulated intensities of a suitable subset of the available spectral lines shown in Table II. We chose for this purpose two neutral copper lines (Cu I at 521.8 nm and Cu I at 578.2 nm) and two lines belonging to different stages of ionization of Ni (Ni II at 241.6 nm and Ni I at 362.0 nm). The network was trained using as inputs the values of the LIBS intensities of the four spectral lines selected and as output the known Ni concentration of the samples. After the training, the ANN model is expected to give the Ni concentration in unknown samples on the basis of the measured LIBS intensities of the same lines used at the training stage.
We used a feed-forward neural network with one hidden layer, to implement the fitting model. The transfer functions for the hidden neurons and the output neurons are, respectively, the usual hyperbolic tangent sigmoid function and linear function, as figure 3 shows. We tried a number of hidden neurons ranging from 3 to 10. For each number of hidden neurons, we performed 10 different experiments by training, validating and testing the network with 70%, 15% and 15%, respectively, of the spectra. The spectra at our disposal were 13000. For each experiment, the network performance was evaluated as the average of the Mean Squared Errors (MSE) made on the test set in the 10 runs. The best performance was achieved with 3 hidden neurons. The parameters used are summarized in Table III.

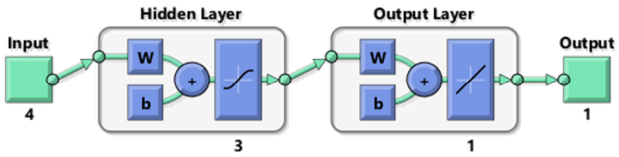

Fig. 3. Network model employed in the experiments. The model has 4 inputs, 3 hidden neurons with hyperbolic tangent sigmoid transfer function, and 1 output neuron with linear transfer function (the figure was depicted in the Matlab® environment).

Table III - Parameters of the neural network model employed

Parameter	Value
Number of hidden layers	1
Number of hidden neurons	3
Transfer functions	Hyperbolic tangent sigmoid (hidden layer), linear (output layer)
Training algorithm	Levenberg-Marquardt
Stopping criterion	1000 interations | gradient < 10^{-5} | after 6 validation failures
Number of input variables	4
Number of output variables	1

Figure 4 shows the regression graphs for the Training, Validation, and Test sets, and the whole data set: the R value = 1 indicates an optimal linear fitting of the model to the data. Indeed, the MSE is of the order of 10^{-4}. Figure 5 shows the error histogram for the Training, Validation and Test sets.

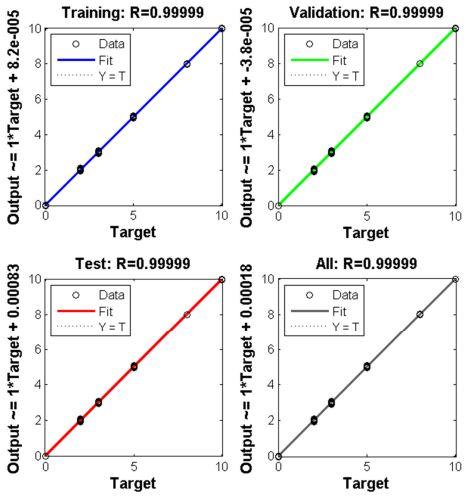

Fig. 4. Regression performance of the ANN predictions with respect to the nominal Ni concentration for Training, Validation and Test sets, and the whole data set. Continuous lines correspond to the ideal condition where the output coincides with target.

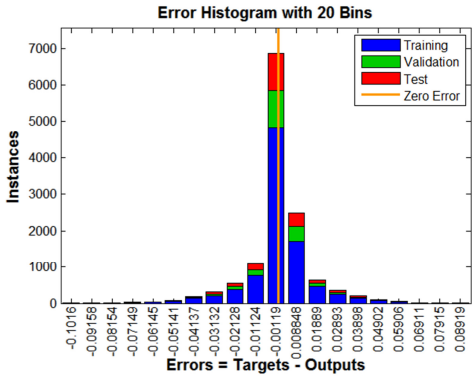

Fig. 5. Error histogram of the ANN predictions with respect to the nominal Ni concentration for Training, Validation and Test sets.

Note that the ANN model correctly predicts the Ni concentration of the test samples independently on the experimental parameters used for the generation of the simulated spectra, in a way very similar to the CF-LIBS approach. However, a more sensible assessment of the ANN performance can be obtained by testing the network on 'unknown' samples that were never used during the training phase. To this purpose, we generated another set of simulated LIBS spectra, roughly corresponding to laser energies of 75 and 125 mJ, as reported in the next table.

Table IV - Parameters used for the generation of the 'unknown' synthetic LIBS spectra

Sample	Laser Energy	[Ni] (%)	T (eV)	n_e (cm^{-3})
S1	75	2.5	1.15	$3.25x10^{16}$
S2	75	5	1.15	$3.25x10^{16}$
S3	75	8	1.15	$3.25x10^{16}$
S4	125	2	1.21	$3.7x10^{16}$
S5	125	4	1.21	$3.7x10^{16}$
S6	125	7	1.21	$3.7x10^{16}$

As done before, 1000 spectra per sample were simulated and used as test of the performance of the ANN.

The results of this test (figure 6) are unsatisfactory. Indeed, the MSE of the ANN predictions on spectra obtained in conditions different from the ones used for the training of the net is of the order of 10^{-1}, showing that the information provided to the ANN is, evidently, not enough to disentangle the complex link between temperature, electron number density, Ni concentration and the LIBS line intensities. Similar results can be obtained using as inputs all the seven spectral lines simulated in the experiment.

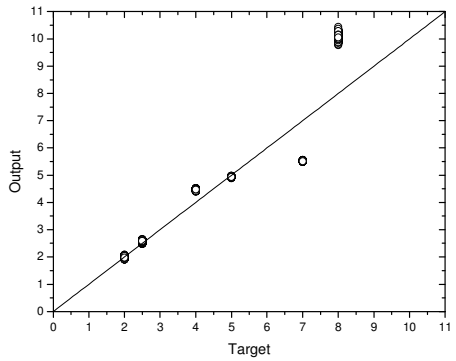

Fig. 6. Comparison between the target values and the neural outputs for the Ni concentrations related to the 'unknown' LIBS spectra corresponding to the parameters in Table IV. Continuous line corresponds to the ideal condition where the output coincides with the target.

The strategy that we applied for improving the ANN performance on 'unknown' samples derives from the results obtained in ref. [19]; in that paper, the authors demonstrated the possibility of training an ANN for determining, using only the spectral information obtained from the LIBS spectrum, the electron temperature and electron number density of the corresponding LIBS plasma. The main issue faced in ref. [19] was the problem related to the acquisition of LIBS spectra with 'known' values of electron temperature and electron number density to be used for the training of the ANN. A feasible solution was found associating to all the spectra acquired in the same experimental conditions the same values of the electron temperature and number density, as previously calculated using the CF-LIBS algorithm on the corresponding averaged spectra. This simplification reduces dramatically the time needed for the preliminary analysis of the samples to be used for the training. The robustness of the ANN algorithm tolerates the intrinsic experimental uncertainty on these parameters and the ANN model created, after the training stage, was demonstrated to give reliable information on the electron temperature and electron number density of unknown spectra, on a single spectrum basis, in fractions of a second. Of course, for the method to be effective, the spectral lines used as inputs for the network must bring the information needed for determining the parameters of the LIBS plasma. Actually, the relative intensities of the lines selected for the previous experiments depend on the electron temperature (that could be calculated from the two neutral copper lines at 521.8 nm and 578.2 nm), while the two Ni lines, belonging to different stages of ionization (Ni II at 241.6 nm and Ni I at 362 nm) would allow the determination of the electron number density. The same lines provide information about the Ni concentration in the samples. Therefore, in this case the outputs of the neural network are the values of the electron temperature and the electron number density (properly rescaled for having all the variables in the same order of magnitude), together with the Ni concentration. The network architecture has been experimentally determined as explained earlier (see figure 7).

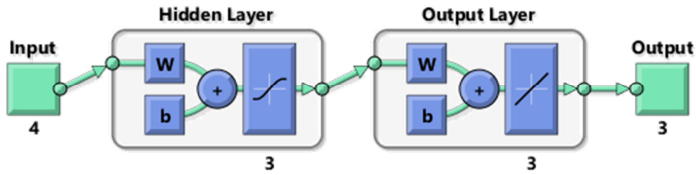

Fig. 7. Improved neural network model employed in the experiments. The model has 4 inputs, 3 hidden neurons with hyperbolic tangent sigmoid transfer function, and 3 outputs with linear transfer function.

As in the previous test, the ANN demonstrates a good ability in reproducing almost perfectly the plasma parameters and Ni concentration, at the three laser energies considered in this paper (see figures 8 and 9). The MSE on Training, Validation and Test sets is of the order of 10^{-4}.

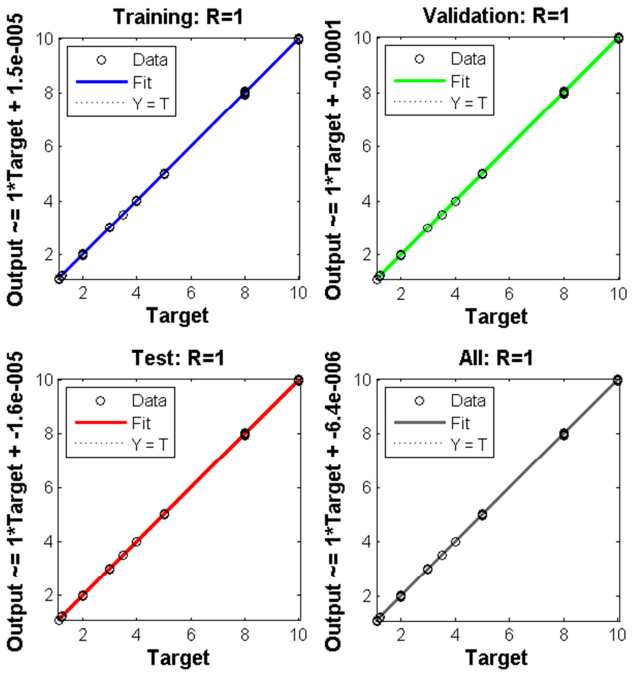

Fig. 8. Regression performance of the improved ANN for Training, Validation and Test sets, and the whole data set.

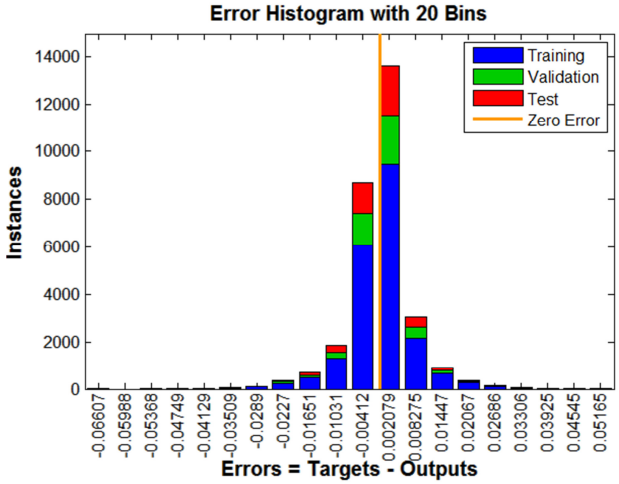

Fig. 9. Error histogram of the improved ANN outputs with respect to the target for Training, Validation and Test sets.

The real test of the performance of the improved ANN exploits a set of samples not used for the training stage. As in the previous case, we used as test set the new set of LIBS spectra simulated using the parameters in Table IV. The results of the analysis are shown in figure 10.

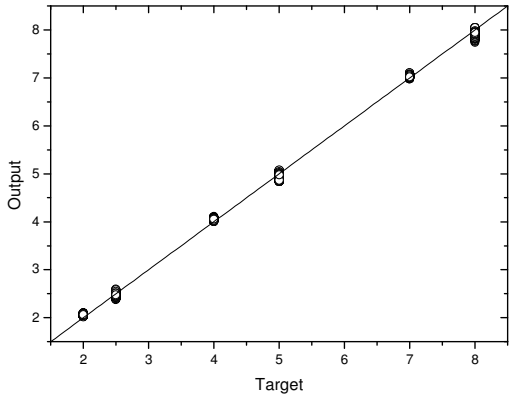

Fig. 10. Comparison between the target values and the output of the improved ANN for the Ni concentration related to the 'unknown' LIBS spectra corresponding to the parameters in Table IV. Continuous line corresponds to the ideal condition where the output coincides with the target.

In this case, the improved ANN is capable of predicting with appreciable precision (MSE of the order of 10^{-3}) the Ni concentration in the 'truly unknown' samples used for the test. One should note that the improved ANN gives also the correct values of the electron temperature and electron number density (with an error around 2%), on a single spectrum base, as shown in figure 11.

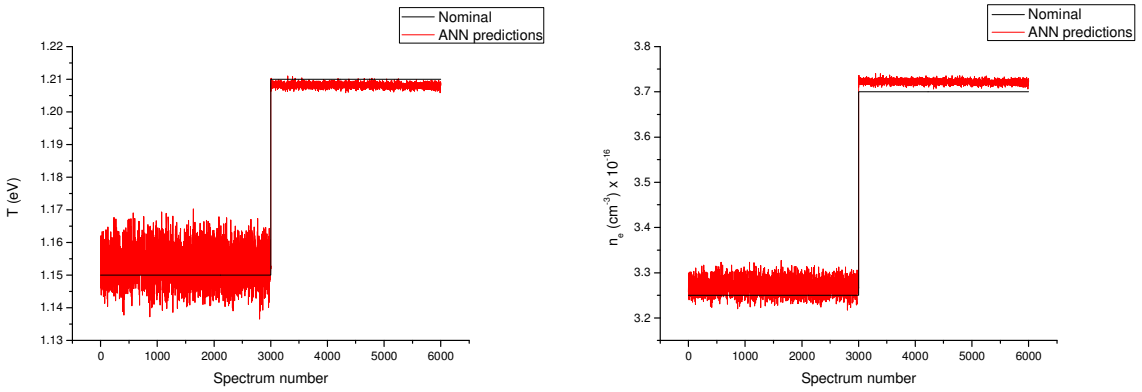

Fig. 11. Predictions of the improved ANN for the spectral parameters of the set of 'unknown' LIBS spectra, corresponding to the parameters in Table IV. Left: Electron temperature; Right: Electron number density. The curve in red represents the predictions of the ANN, the one in black the nominal value of the parameters. Each point corresponds to a single LIBS spectrum.

4 – Conclusion

In this paper we have demonstrated that in the presence of large variations, either wanted or undesired, of the laser beam energy or of its coupling with the sample, an approach based on the use of a single calibration curve might not be appropriate. Using a set of simulated LIBS spectra, synthetized assuming different experimental parameters (electron temperature, electron number density and ablated mass) we have also shown that a 'general purpose' approach based on the application of a simple ANN, having as inputs the LIBS line intensities, might have a poor precision in predicting the Ni concentration on a Cu matrix. However, a hybrid approach where the ANN is trained using the results of a CF-LIBS calculation of the electron temperature and electron number densities (on the averaged spectra) has demonstrated to be much more precise, giving as fringe benefit also a good information on the electron temperature and electron number densities on the unknown samples, on a single spectrum base, as in CF-LIBS analysis but in a much faster way. These results underline the importance to deal with the mathematical aspects of the ANN method without forgetting the physical principles at the basis of the LIBS technique, when the objective is using the ANN technique for 'real world' applications.

References

[1] Haykin, S.S., *Neural networks. A comprehensive foundation*, Second Edition, Prentice-Hall, New Jersey, U.S (1999).

[2] Kuncheva, L.I., *Combining pattern classifiers: Methods and algorithms*, Wiley Interscience, New Jersey, U.S. (2004).

[3] Miziolek, A., Palleschi, V., Schechter, I., *Laser Induced Breakdown Spectroscopy*, Cambridge University Press, Cambridge (2006)

[4] Winefordner, J.D., Gornushkin, I.B., Correll, T., Gibb, E., Smith, B.W., Omenetto, N., Comparing several atomic spectrometric methods to the super stars: Special emphasis on laser induced breakdown spectrometry, LIBS, a future super star, *J. Anal. Atom. Spectrom.* 19 (9) (2004)1061-1083.

[5] Caceres, J.O., Moncayo, S., Rosales, J.D., De Villena, F.J.M., Alvira, F.C., Bilmes, G.M., Application of laser-induced breakdown spectroscopy (LIBS) and neural networks to olive oils analysis, *Appl. Spectrosc*. 67 (9) (2013) 1064-1072.

[6] Boueri, M., Motto-Ros, V., Lei, W.-Q., Ma, Q.-L., Zheng, L.-J., Zeng, H.-P., Yu, J., Identification of polymer materials using laser-induced breakdown spectroscopy combined with artificial neural networks, *Appl. Spectrosc.* 65 (3) (2011) 307-314.

[7] El Haddad, J., Bruyère, D., Ismaël, A., Gallou, G., Laperche, V., Michel, K., Canioni, L., Bousquet, B., Application of a series of artificial neural networks to on-site quantitative analysis of lead into real soil samples by laser induced breakdown spectroscopy, *Spectrochim. Acta B* 97 (1) (2014) 57-64.

[8] Vítková, G., Novotný, K., Prokeš, L., Hrdlička, A., Kaiser, J., Novotný, J., Malina, R., Prochazka, D., Fast identification of biominerals by means of stand-off laser induced breakdown spectroscopy using linear discriminant analysis and artificial neural networks, *Spectrochim. Acta B* 73 (2012) 1-6.

[9] D'Andrea, E., Pagnotta, S., Grifoni, E., Lorenzetti, G., Legnaioli, S., Palleschi, V., Lazzerini, B., An Artificial Neural Network approach to Laser-Induced Breakdown Spectroscopy Quantitative Analysis, *Spectrochim. Acta B* (2014), doi: 10.1016/j.sab.2014.06.012.

[10] Mikut, R., Reischl, M., Data mining tools, WIREs Data Mining and Knowledge Discovery, John Wiley & Sons, Inc. (2011).

[11] Rumelhart, D.E., Hinton, G.E., Williams, R.J., Learning representations by back-propagating errors, *Nature* 323 (1986) 533–536.

[12] Palleschi, V., Comment on "a multivariate model based on dominant factor for laser-induced breakdown spectroscopy measurements" by Zhe Wang, Jie Feng, Lizhi Li, Weidou Ni and Zheng Li, J. Anal. At. Spectrom., 2011, DOI: 10.1039/c1ja10041f, *J. Anal. Atom. Spectrom.* **26** (11) (2011) 2300-2301.

[13] Andrade, J.M., Cristoforetti, G., Legnaioli, S., Lorenzetti, G., Palleschi, V., Shaltout, A.A., Classical univariate calibration and partial least squares for quantitative analysis of brass samples by Laser-Induced Breakdown Spectroscopy, *Spectrochim. Acta B* **65** (8) (2010) 658-663.

[14] International Union of Pure and Applied Chemistry, Guidelines for calibration in analytical chemistry, Part 1. Fundamentals and single component calibration, *Pure & Appl. Chem*. **70** (4) (1998) 993-1014.

[15] Ciucci, A., Corsi, M., Palleschi, V., Rastelli, S., Salvetti, A., Tognoni, E., New Procedure for Quantitative Elemental Analysis by Laser-Induced Plasma Spectroscopy, *Appl. Spectrosc.*, 53 (1999) 960-964.

[16] Cremers, D.A., Radziemski, L.J., LIBS Analytical Figures of Merit and Calibration in *Handbook of Laser-Induced Breakdown Spectroscopy, Second Edition*, John Wiley & Sons Ltd, Oxford, UK (2013).

[17] Tognoni E., Cristoforetti G., Legnaioli S., Palleschi V., Calibration-Free Laser-Induced Breakdown Spectroscopy: State of the art, *Spectrochim. Acta B 65* (2010) 1-14.

[18] Cavalcanti, G.H., Teixeira, D.V., Legnaioli, S., Lorenzetti, G., Pardini, L., Palleschi, V., One-point calibration for calibration-free laser-induced breakdown spectroscopy quantitative analysis, *Spectrochim. Acta B* **87** (2013) 51-56.

[19] Borges, F.O., Cavalcanti, G.H., Gomes, G.C., Palleschi, V., Mello, A., A fast method for the calculation of electron number density and temperature in laser-induced breakdown spectroscopy plasmas using artificial neural networks, *Appl. Phys. B*. (2014) DOI:10.1007/s00340-014-5852-8

[20] Bredice, F., Borges, F.O., Sobral, H., Villagran-Muniz, M., Di Rocco, H.O., Cristoforetti, G., Legnaioli S., Palleschi, V., Salvetti, A., Tognoni, E., Measurement of Stark broadening of Mn I and Mn II spectral lines in plasmas used for Laser-Induced Breakdown Spectroscopy, *Spectrochim. Acta B* **62** (2007) 1237–1245.

[21] Cristoforetti, G., De Giacomo, A., Dell'Aglio, M., Legnaioli, S., Tognoni, E., Palleschi, V., Omenetto, N., Local Thermodynamic Equilibrium in Laser-Induced Breakdown Spectroscopy: Beyond the McWhirter criterion, *Spectrochim. Acta B* **65(1)** (2010) 86-95.

[22] NIST database: http://physics.nist.gov/cgi-bin/AtData/main_asd